Optimization of off-axis electron holography performed with femtosecond electron pulses

Florent Houdellier, Giuseppe Mario Caruso, Sébastien J. Weber, M.J. Hÿtch, Christophe Gatel, Arnaud Arbouet

Optimization of off-axis electron holography performed with femtosecond electron pulses

F. Houdellier[a,1], G.M. Caruso[a], S. Weber[a], M. J. Hÿtch[a], C. Gatel[a], A. Arbouet[a,1],

[a] *CEMES-CNRS, Université de Toulouse, Toulouse, France*

Abstract

We report on electron holography experiments performed with femtosecond electron pulses in an ultrafast coherent Transmission Electron Microscope based on a laser-driven cold field emission gun. We first discuss the experimental requirements related to the long acquisition times imposed by the low emission/probe current available in these instruments. The experimental parameters are first optimized and electron holograms are then acquired in vacuum and on a nano-object showing that useful physical properties can nevertheless be extracted from the hologram phase in pulsed condition. Finally, we show that the acquisition of short exposure time holograms assembled in a stack, combined with a computer-assisted shift compensation of usual instabilities encountered in holography, such as beam and biprism wire instabilities, can yield electron holograms acquired with a much better contrast paving the way to ultrafast time-resolved electron holography.

Keywords: Ultrafast Transmission Electron Microscopy, electron holography, cold field emission, femtosecond laser,

1. Introduction

Off-axis electron holography in a Transmission Electron Microscope is a well-established interferometric method yielding quantitative maps of electric, magnetic, and strain fields at the nanoscale [1]. A coherent electronic wave that has interacted with a sample (object wave) is interfered with the part of the beam that has gone through the vacuum (reference wave) thanks to an electrostatically charged wire or so called Möllenstedt biprism. The resulting interference pattern (*i.e.* the hologram) contains all information on the phase shift of the electron wave resulting of its interaction with the local fields [2]. To extract quantitative phase and amplitude values of the hologram, the well known Fourier filtering method can be implemented [3, 4]. Bright field electron holography can be used to map the sample thickness [5], the mean inner potential of a sample [6], the electrostatic field [7] as well as the magnetic field [8] with sub nanometric resolution. More re-

cently, it has been shown that electron holography allows the charge on individual nanoparticles to be measured to a precision of one elementary unit of charge [9] or monitor in-situ the field emission from carbon cone nanotips[10]. In addition, based on the interference of one diffracted beam originating from two areas with different strain states, dark-field electron holography allows mapping the strain field with nanometer scale spatial resolution[4].

Since 2005, the development of ultrafast Transmission Electron Microscopes (UTEM) has enabled TEM studies with both atomic scale spatial resolution and sub-picosecond temporal resolution[11, 12]. Today, most imaging and diffraction techniques have been endowed with the temporal dimension thanks to time-resolved optical pump-electron probe experiments. Recently, electron holograms have been acquired with femtosecond electron pulses in UTEMs based on laser triggered nanosized emitters[13, 14]. However, ultrafast electron holography is still at the early stage due to a combination of instrumental and methodological challenges mainly caused by the low current available in these instruments [15].

In this work, we report on the development and optimisation of electron holography experiments acquired with femtosecond electron pulses in a recently developed UTEM based on a laser-driven cold field emission gun [14]. We first present briefly the experimental setup before discussing the phase detection limit of an electron hologram acquired using the coherent UTEMs. We show why the low electron probe current available in the laser driven nanoemitter technology leads to severe difficulties especially from the need to increase the exposure time required for the acquisition of exploitable electron holograms. We then optimize the experimental parameters to maximize the contrast of the hologram fringes acquired with femtosecond electron pulses. In these optimized conditions, the phase of electron holograms acquired on a test sample of magnesium oxyde nanocubes can be retrieved and reveals the usual contribution of the mean inner potential of the nano-objects. Finally, we also show how the effect of instabilities inherent to the long acquisition times can be minimised. Altogether these results pave the way to ultrafast time-resolved electron holography.

2. High-brightness Ultrafast Transmission Electron Microcoscope based on a laser-driven cold field emission gun

Our experiments have been performed on a recently developed ultrafast Transmission Electron Microscope (UTEM) based on a laser-driven cold field emission gun. Our UTEM is a modified HF 2000, a 200keV CFEG-TEM from Hitachi High Technologies already described in previous publications [16, 14, 15]. Figure 1 -a) shows the outline of this unique instrument .

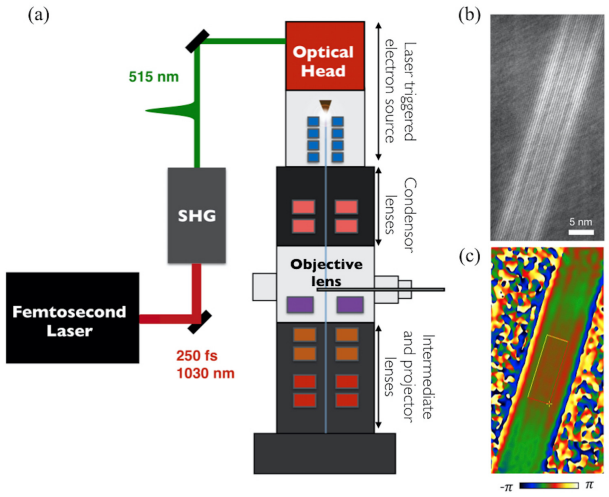

Figure 1: (Color Online) a) Principle of the coherent Ultrafast Transmission Electron Microscope. A femtosecond laser beam triggers the emission of electrons from the apex of a tungsten nanotip located inside a 200keV cold-field emission gun. b) Electron hologram acquired in vacuum using this new coherent UTEM. c) Hologram phase extracted from the hologram reported in b).

Briefly, our optical set-up is based on an amplified fiber laser yielding femtosecond infrared pulses (250 fs, 1030 nm) at a tunable repetition rate (single shot to 40 MHz). The infrared laser beam is first sent onto a nonlinear crystal (BBO) in which 515 nm femtosecond laser pulses are generated by second-harmonic generation (SHG). The visible ultrashort laser pulses are then sent into an optical head which gathers all optical components to adjust the power, polarization and steer the laser beam onto the nanoemitter. The latter is a monocrystalline tungsten $< 310 >$ oriented tip typical in cold-field emission guns. The laser beam is finally focused onto the nanotip apex inside the electron source by the combination of a plane mirror and a parabolic mirror (f=8 mm) triggering the electrons pulses [16]. The tight focusing of the laser beam at the apex combined with the optical field enhancement confines the emission of the electrons to a small region of the emitter yielding a large brightness [17, 13, 14]. In the experiments reported below, the extraction voltage is set at 4 kV, a value below the voltage threshold necessary to trigger continuous emission but selected to properly focus the electrons probe, and the gun ratio is set in virtual cross over mode (R=5) [14]. The UTEM was operated at an acceleration voltage of 150 kV . The electron biprism is an homemade 400nm thick quartz fiber coated with gold and located slightly above the selected area plane of the TEM. The camera used to acquire the holograms is a conventional 4k4k Charged Coupled Device (CCD) USC1000 by Gatan, and the holograms are post processed using home made scripts written in Digital Micrograph scripting language. The repetition rate of the laser and therefore of the electron beam is 2 MHz. An incident laser intensity in the 4-7 mW range at the entrance of the electron gun typically yields a probe current in the 0.5-4 pA range which correspond to 1.5-12 electrons per pulse at the sample plane. The number of electron per pulse is therefore kept at a low value to minimize the Coulomb repulsion among the electrons inside a given pulse. In this so-called single electron regime, the spectral and temporal broadening of the electron pulses remains negligible.

In the following experiments, the electron pulses have a spectral width of approximately 1 eV and a FWHM time duration of 400 fs at the sample

measured by pump-probe electron energy gain spectroscopy (EEGS) experiments [18],[19]. As will be discussed in the next part, the low current available in UTEMs compared to standard continuous Field Emission TEM has important consequences on the detection limit in electron holography performed with these instruments.

3. Detection limits in off-axis electron holography with femtosecond electron pulses

Figure 1 -b) and -c) respectively show an ultrafast electron hologram and the associated reconstructed phase. The phase noise, defined as the standard deviation of the phase in the vacuum, is strongly influenced by several key experimental parameters. Assuming that the arrival of electrons is Poisson distributed, resulting in *shot noise* [20], the standard deviation of the reconstructed phase can be written as [21, 20]:

$$\sigma_\phi = \sqrt{\frac{2}{DQE \cdot C^2 \cdot N_{epx}}}. \quad (1)$$

C is the fringes contrast of the hologram. N_{epx} is the number of electrons per pixel and DQE is the detective quantum efficiency of the detector used to record the hologram. The hologram figure of merit can alternatively be quantified by the *phase detection limit*, *i.e.* the smallest detectable phase difference [22]:

$$\delta\phi = SNR\sqrt{\frac{2}{DQE \cdot C^2 \cdot N_{epx}}} \quad (2)$$

where the desired signal-to-noise ratio SNR is a given parameter. To properly determine the result of an experiment without ambiguity, it is generally admitted that a SNR between 3 and 10 is necessary [15].

As presented in equation 2 , the fringe contrast contributes more strongly to the phase detection limit compared to the other parameters. Effect of external perturbations can be introduced through their influence on the contrast. Furthermore, in addition to the experimental set-up instabilities, the hologram contrast is also affected by the partial coherence of the electron source, by inelastic interactions of the electron beam inside the specimen and by the Modulation Transfer Function (MTF) of the detector for a given interfringe distance s. A useful expression of the contrast used to take into account all these contributions is :

$$C = C_{coh}C_{inel}C_{inst}MTF \quad (3)$$

where C_{inst}, C_{inel} and C_{coh} correspond to the influence of instabilities, inelastic scattering and partial coherence, respectively [22]. C_{inst}, unlike the other parameters, depends on the exposure time. It is commonly accepted that contrast values better than 15% are required to extract a phase with enough signal-to-noise ratio and good spatial resolution.

In the context of ultrafast TEM experiments, the number of electrons per pixel in equation (2) can be determined by the relation:

$$N_{epx} = N_{ppx} \cdot f \cdot t_{exp} \quad (4)$$

where f is the laser repetition rate, t_{exp} the ex-

posure time and N_{ppx} the number of electrons per pulse per pixel which can be expressed by the number of electrons per pulse N_{epp} in the electron probe divided by the total number of pixel in the measurement area N_{px}. Substituting equation (4) in equation (2), we obtain:

$$\delta\phi = \frac{SNR}{C_{coh}\, C_{inst}\, MTF}\sqrt{\frac{2\, N_{px}}{DQE\, N_{epp}\, f\, t_{exp}}} \quad (5)$$

where the contrast C has been expressed as in equation (3), assuming the contribution of inelastic scatterings to be negligible. Equation (5) highlights the different parameters affecting the contrast of holograms acquired with femtosecond laser pulses in a UTEM. In the following we will discuss how the phase detection limit could be optimized by adjusting these various parameters.

4. Optimisation of the experimental parameters for electron holography with femtosecond electron pulses

4.1. Number of electrons per pulse and repetition rate

Using standard continuous cold field emission source, emission current in the microampere range is usually obtained in the tip area, while it remains limited in the picoampere range in laser-driven mode. It is clear from equation (1) that this drop by approximately six orders of magnitude of the emission and, as a consequence, probe current between DC and laser-driven mode under the same electron optical conditions has a strong influence in the phase detection limit of electron hologram acquired with pulsed electrons source.

It is possible to adjust the number of electrons per pulse, N_{epp} by changing the laser power. However, this is limited for two reasons. First, the laser intensity incident on the nanoemitter is limited by the cathode damage threshold. This limits the number of electrons that can be extracted from the tungsten nanotip without deteriorating it [16]. Second, as discussed previously, the excellent spatio-temporal resolution of UTEMs is a direct consequence of the low number of electrons in each pulse. Increasing the latter promotes space-charge effects leading to spectral and temporal broadening of the electron pulse.

The range over which the laser repetition rate f in equation (5) can be adjusted is also limited. First, in UTEMs, the low number of electrons per pulse imposes experiments to be carried out in stroboscopic mode where the information is accumulated over billions of excitation-detection cycles. These stroboscopic experiments demand the physical system under scrutiny to be fully relaxed before the advent of the following excitation [15]. This condition then limits the laser repetition rate to values compatible with the system dynamics. Second, increasing the repetition rate above a certain threshold would require a decrease in the laser intensity on the nanoemitter to avoid its destruction by cumulative heating. The benefit of a higher repetition rate would therefore be cancelled by a de-

crease in the number of electrons per pulse.

4.1.1. Spatial coherence

The upper limit for the fringe contrast is set by the spatial coherence which is in turn limited by the source brightness. This explains the choice of developing a UTEM based on cold-field emission to optimise the source brightness for electron holography experiments. Indeed, our instrument has been shown to have the highest brightness of all UTEMs in the $10^7 - 10^8$ $\mathrm{Am^{-2}Sr^{-1}}$ range at 1 Mhz of Laser repetition rate [14]. As is routine for conventional electron holography we have further optimized the coherence length in the beam overlap direction, *i.e.* perpendicularly to the biprism wire by using an elliptical illumination [22].

This condition is used to demagnify strongly the effective source size in the direction perpendicular to the biprism wire and then maximise the spatial coherence length along the interference direction. However, an optimum elliptic ratio needs to be used to avoid serious loss of number of electrons per pixel and then preventing a too large increase of the exposure time. Like in standard off-axis electron holograpy the optimum ratio between the minor and the major axis of the ellipse is around 0.1 [1].

4.2. Acquisition time

The benefit of increasing exposure time is eventually counteracted by instrumental instabilities. In conventional electron holography, the optimum exposure time can be predicted based on the hologram characteristics (fringe spacing, interference width and pixel size) and instabilities [23]. However, due to the low current available in our UTEM much longer acquisition times are unfortunately required compared to usual reported situations. Indeed, whereas a few seconds are typically used for experiments requiring a high S/N ratio with continuous electron beams, exposure times of several tens of seconds were necessary with our instrument. For example, as can be seen from Figure 2, the contrast of the hologram recorded with 10 s of exposure time and 30 V of biprism voltage is too weak to reconstruct a phase with enough signal-to-noise ratio.

Longer exposure times increase the number of electrons dose per pixels and therefore the hologram contrast as long as conditions are sufficiently stable. In Figure 2 (c) the lowest reconstructed phase standard deviation is obtained for $t_{exp} = 100$ s. In our experiments, exposure times between 100 and 150 s have consistently yielded the best results depending on microscope environment stability.

4.3. Biprism voltage

The choice of the optimal biprism voltage usually depends on the size of the overlap region related to the distance between the reference and the sample areas, and the required spatial resolution of the reconstructed phase, the latter being related to the fringe spacing. Systematic experiments performed

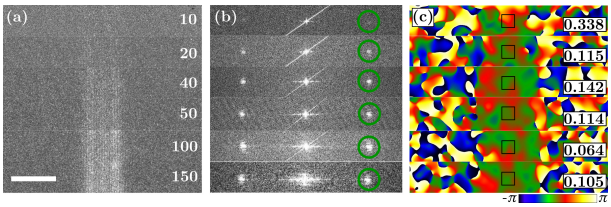

Figure 2: (Color Online) Influence of the exposure time on the hologram. (a) Electron holograms acquired in vacuum. Exposure times in seconds are displayed in white. Scale: 5 nm. (b) Power spectrum (square of the Fast Fourier Transform) of the holograms. Green circles indicate the mask position in the Fourier space. The achieved spatial resolution is 2 nm. (c) Reconstructed phases. Standard deviations calculated inside the black square are displayed. Experimental conditions: biprism voltage 30 V, W_{LAS} = 8 mW, f = 2 MHz, $N_{epp} \sim 9$, binning 1, magnification 200 kX.

with an acquisition time of 150 s have shown that the range of usable biprism voltages is more limited than using the conventional DC emission source under the same optical conditions. As we can see in Figure 3 (c), it is possible to extract phases with a rather low standard deviation for low biprism voltages (15 V - 20 V). However, in these cases the hologram field of view are too small to be useful in practice. Unfortunately, the contrast of the hologram drops dramatically for biprism voltages larger than 35 V.

This can be explained by the fact that due to smaller fringe separation, the hologram contrast becomes more sensitive to the instabilities using 150 s of acquisition time (in addition to the effect of the CCD camera MTF). Increasing the biprism voltage above 35V would mean decreasing the exposure time but, as already showed in Figure 3, this will not improve the phase standard deviation. Our results show that, using an exposure time of 150 s and a magnification of 200 kX, the set of useful biprism voltages remains limited to the 20 V - 32 V range.

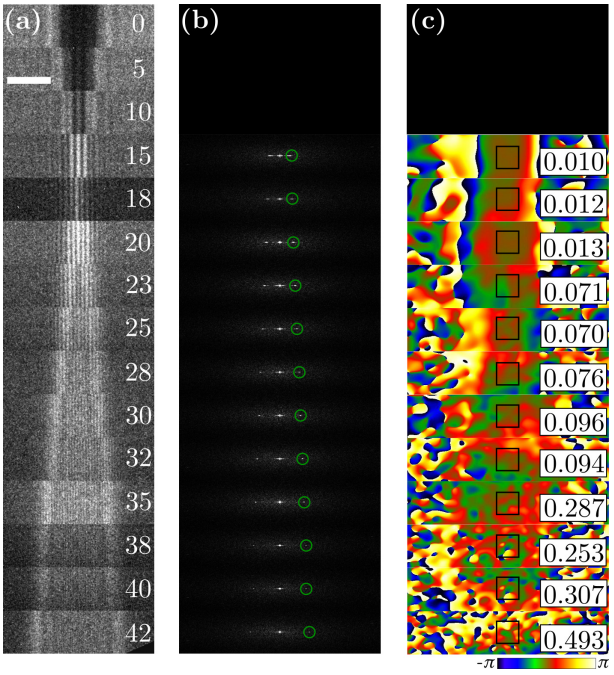

Figure 3: (Color Online) Hologram acquired as a function of the the biprism voltage. (a) Electron holograms acquired in vacuum. Biprism voltages in volts are displayed for each case. Scale: 15 nm. (b) Holograms power spectrum. The green circles represent the 2 nm resolution mask in the Fourier space. (c) Reconstructed phases. Standard deviations calculated inside the black square are displayed. Experimental conditions: exposure time 150 s, W_{LAS} = 7.5 mW, f = 2 MHz, $N_{epp} \sim 12.5$, binning 1. Magnification: 200 kX

4.4. Electron holography with femtosecond electron pulses on MgO nanocubes

Using optimum values of exposure time and biprism voltage determined previously, we have acquired off-axis holograms with ultrashort electron pulses on a magnesium oxide (MgO) cube as a test sample. The raw datas and the phase reconstruction process are reported in Figure 4.

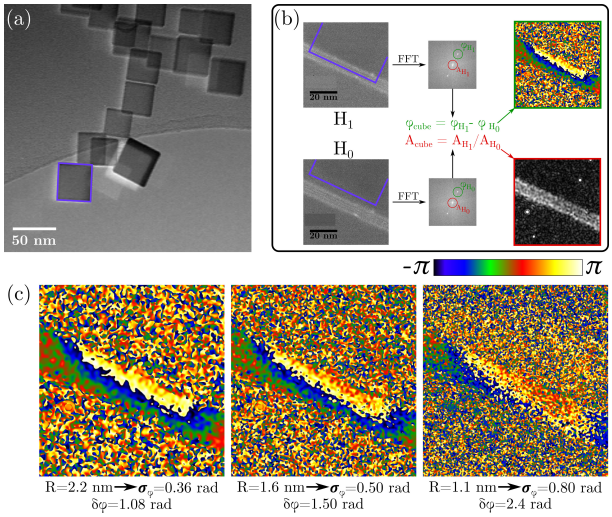

Figure 4: (Color Online) MgO cube phase reconstruction performed with holograms acquired using ultrashort electron pulses. (a) TEM micrograph of MgO cubes deposited on a carbon foil. (b) Standard phase and amplitude reconstruction process using the specimen and reference holograms [1]. The purple square stands for the precise localisation of the MgO cube relatively to the hologram area. A phase jump of 5 rad si measured due to the 13 V MgO mean inner potential contribution. (c) Effect of the mask size used in Fourier space to retrieve the electrostatic phase with a resolution R. The phase standard deviation is reported for each resolution as well as the phase detection limit. Phase detection limits are calculated under ideal conditions ($SNR = 3$, $C_{inst} = 1$). Experimental conditions: biprism voltage 28 V, exposure time 150 s, $W_{LAS} = 8$ mW, $f = 2$ MHz, $N_{epp} \sim 8$, binning 1. Magnification: 200 kX Electron dose : $10e^-/\mathring{A}^2$

Figure 4(b) shows the standard reconstruction steps used in the hologram phase analysis. H_1 corresponds to the MgO cube hologram and H_0 is the reference hologram acquired without specimen. The reconstructed phase of the specimen reported inside the green square has been obtained after substraction of the phase extracted from reference hologram to remove all the various distorsions of the experimental setup. Despite the limitations originating from the use of ultrashort electron pulses, we can clearly see the phase change from the MgO mean inner potential.

Figure 4 (c) shows the effect of the mask size (*i.e.* the phase spatial resolution) on the reconstructed phase. Increasing the mask size in Fourier space improves the spatial resolution of the phase image R at the expense of the phase standard deviation, as reported in Figure 4 (c). A spatial resolution of 2nm is possible.

5. Maximizing the signal-to-noise ratio of holograms phases acquired with femtosecond electron pulses in low-dose-like conditions: images stack and fringe drift correction.

We have seen that despite the high brightness of our electron source, off-axis electron holography remains a challenge. Indeed, the low probe current available in our coherent UTEM must be compensated by long acquisition times which make our experiments much more sensitive to instabilities than

conventional electron holography.

In this section we will show how the use of image stacks previously introduced in conventional holography experiments [24, 25], can contribute to overcome this limitation.

The idea is that each individual hologram in the stack is recorded using short exposure times below the threshold of various instabilities. However, a mere summation of the collected individual holograms will not improve the final contrast. Indeed, the result will be equivalent to a single hologram acquired with a total exposure time equal to the sum of each individual exposure time. In order to properly exploit the benefit of hologram stack to remove the effect of instabilities, a numerical post-processing for fringe drift compensation is required before performing the final sommation between each individual hologram [24].

We have used the approach for electron holograms acquired with femtosecond electron pulses. Data processing has been performed using homemade scripts in Digital Micrograph. We have first developed an automatic acquisition procedure of the hologram stack where the acquisition time of the whole stack corresponds to the targeted exposure time. Regarding the data treatment, a first operation is primarily carried out to remove dead pixels (which can originate from Xrays events, errors in the gain or dark references of the CCD camera) . These pixels, with abnormal intensities, are detected in each individual hologram of the stack and then replaced with the average intensity of the adjacent pixels in order to avoid any artefact in the phase reconstruction.

The next steps are the numerical fringe drift compensation and the final phase reconstruction. Fringes drift can be induced either by mechanical instabilities as well as microscope electronic instabilities which could lead to random tilt or shift of the incoming electron beam. A first rough alignement is performed after applying a spatial filter to remove the holographic fringes while keeping the Fresnel fringes. A cross-correlation procedure is then applied to align each individual hologram with one selected hologram in the stack. A second drift compensation is performed on the resulting stack by measuring the displacement of holographic fringes in term of phase shift. To do so, an average profile of the fringes is extracted for each individual hologram. 1D phase shift is then extracted using a Fourier approach, as for a standard 2D hologram. This phase shift is compared with one selected as a reference and then converted into a number of pixels used to realign each individual hologram relatively to the reference one. Once completed these alignment processes, all the individual drift corrected holograms are finally summed up.

Figure 5 shows the correction effect for two different biprism voltages.

In the *Not corrected* row, individual holograms in the stack have been summed without applying any

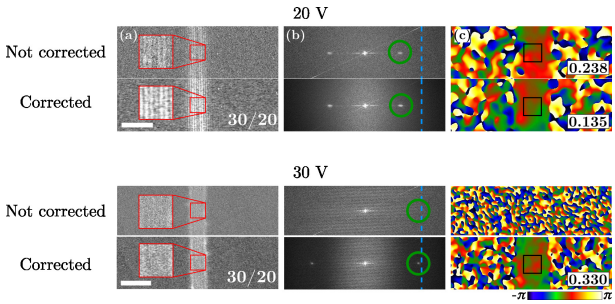

Figure 5: (Color Online) Comparison between holograms obtained after summing all individual holograms in the same stack with (corrected) and without (not corrected) instabilities correction. The experiment has been performed for two different biprism voltages. (a) The two numbers indicate respectiveley the number of individual holograms acquired in the stack and their acquisition time (displayed in second). In the 20 V and 30 V holograms the scales bars are 10 and 20 nm, respectively. The total exposure is 600s (10mn)(b) Power spectrum of the final hologram. The green circles display the 2.5 nm resolution mask in the Fourier space. The blue dashed line shows the position of the spatial frequency $(4.pixels)^{-1}$ (c) Reconstructed phases from the final hologram. Standard deviations calculated inside the black square are displayed. Experimental conditions:W_{LAS} = 8 mW, f = 2 MHz, $N_{epp} \sim 6$, binning 2. Magnification: 200 kX.

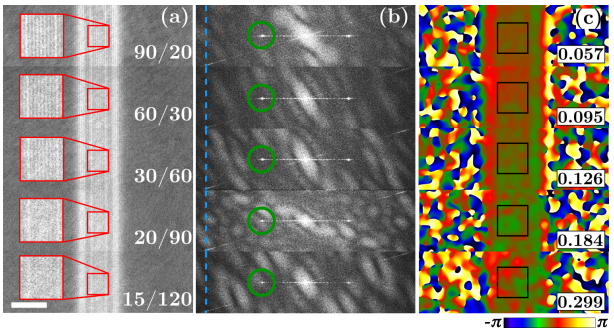

Figure 6: (Color Online) Effect of individual hologram exposure time in summed corrected hologram stacks. (a) The two numbers indicate respectively the number of images in the stack and their individual acquisition time (displayed in second). The total exposure time remains constant (1800s, 30min). The fringe contrast calculated in the optimum hologram (90/20) is 15 %. Scale bars: 10 nm. (b) Power spectrum of the final holograms. The green circles represent the 2.5 nm resolution mask in Fourier space.The blue dashed line shows the position of the spatial frequency $(4.pixels)^{-1}$. (c) Reconstructed phases from the final hologram. Standard deviations calculated inside the black square are displayed. Experimental conditions: W_{LAS} = 8 mW, f = 2 MHz, $N_{epp} \sim 6$, binning 2. Magnification: 400 kX. Biprism voltage: 30 V.

corrections. At low biprism voltages, the effect of instabilities is less problematic than using higher voltages as already discussed in previous paragraph. Phase reconstruction of non corrected hologram can be even possible in this case. However, applying the instabilities correction improves the fringe contrast and strongly reduces the phase noise. The standard deviation is improved by approximately a factor 2. The need to apply drift corrections becomes mandatory at higher biprism voltages. For instance, in the 30 V case without correction no sidebands are detected in the power spectrum precluding the hologram phase retrieval.

Figure 6 shows the effect of the individual hologram exposure time and thus displays the acquisition time threshold from which a loss of fringes contrast due to instabilities can be detected. A total exposure time of 1800 s is kept constant. We can clearly see that, increasing the individual acquisition time will increase the effect of instabilities and then decrease the final fringe contrast. As a consequence, the standard deviation of the associated reconstructed phases increases (Figure 6 (a) and (c)). Therefore, stacks composed of a high number of individual holograms acquired with shorter exposure times should be preferably used to optimise the final hologram contrast.

Nevertheless, there is a limit to how short the individual exposure times can be. The hologram contrast is not sufficient for the algorithm to be used properly for individual exposure times of a few sec-

onds. Individual acquisition times between 20 and 30 s seem to be optimal (as already reported in Figure 2).

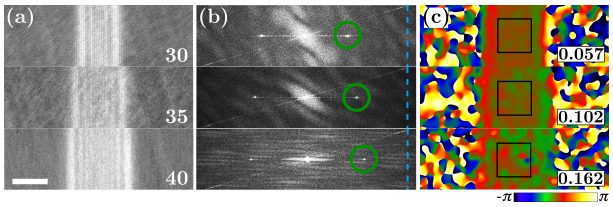

Figure 7: (Color Online) Final summed corrected hologram obtained for different biprism voltage. (a) The numbers indicate the biprism voltage (in volts). Scale: 10 nm. (b) Power spectrum of the final holograms. The green circles represent the 2.5 nm resolution mask in the Fourier space. The blue dashed line shows the position of the spatial frequency $(4.pixels)^{-1}$. (c) Reconstructed phases from the final hologram. Standard deviations calculated inside the black square are displayed. Stacks of 90 individual holograms acquired with 20 s of exposure time. Experimental conditions: $W_{LAS} = 8$ mW, $f = 2$ MHz, $N_{epp} \sim 6$, binning 2. Magnification: 400 kX.

In Figure 7 three summed corrected holograms are displayed for three different biprism voltages. By comparing the final holograms acquired under the same electron optical conditions but with a different total exposure time (150 s for the single not-corrected hologram and 20 s for each of the 90 holograms composing the stack), there is an improvement of 40% and 64% of their phase standard deviations for the 30 and 35 V case, respectively. Moreover, we can notice that using 40 V of biprism voltage the standard deviation obtained using the corrected stack method is even smaller than the value obtained for the 35 V case with $t_{exp} = 150$ s using the same spatial resolution in the reconstructed phase as already reported in Figure 3. The use of hologram stacks enables higher biprism voltages and wider overlap regions.

6. Conclusion

We have discussed the requirements to perform off-axis electron holography with an ultrafast electron beam. The low probe current in the CFEG-UTEM, which is 6 order of magnitude smaller than the one extracted from a continuous CFE source, is the main obstacle. In order to acquire an exploitable hologram from which an useful phase can be extracted, acquisition times between 100 and 150 s are needed. However, in these conditions, the mechanical and electrical instabilities of the microscope cause a dramatic deterioration on the fringe contrast. They further limit the range of usable biprism voltages and with it the field of view which can be mapped. The optimization of the experimental parameters has been done allowing to record electron holograms on a nano-object and reveal the interaction of the electron wave with the mean inner potential of the nano-object. The hologram contrast can be further improved by using image stacks consisting in the sequential acquisition of a high number of individual holograms with an optimum low exposure time lying in the 20 -30 s range chosen to be small enough avoiding strong instabilities contribution, but high enough allowing a phase to be extracted necessary to perform a proper alignement process. Indeed, the hologram stacks are then post-processed applying numerical fringe drift compensation which finally allowed us to increase the

effective acquisition time and improve significantly the signal-to-noise ratio of the reconstructed phase. From a more general point of view, the development of ultrafast electron holography will greatly benefit from the the automation of the electron microscope for the alignment, hologram acquisition and drift correction. For instance, real-time correction algorithms based on the compensation of the hologram fringe drift using the gun tilt coils will be implemented in the future[25]. The future transfer of our technology from the old HF2000 to a recent state-of-the-art TEM, will give us the possibility to move towards this direction and the use of direct electron camera providing a higher DQE should also strongly improve the live-correction process.

7. Acknowledgements

The authors thank the *Institut de Physique du CNRS* and *Agence Nationale de la Recherche* for financial support (ANR grant ANR-14-CE26-0013). This work was supported by *Programme Investissements d'Avenir* under the program ANR-11-IDEX-0002-02, reference ANR-10-LABX-0037-NEXT (*MUSE* grant). This work was supported by the computing facility center CALMIP of the University Paul Sabatier of Toulouse. The authors acknowledge financial support from the European Union under the Seventh Framework Program under a contract for an Integrated Infrastructure Initiative (Reference 312483-ESTEEM2). The authors are grateful to M. Kociak and M. Pelloux for their contribution to the light injector design and fabrication, M. Kociak and E. Snoeck for their support.

References

[1] Edgar Völkl, Lawrence F. Allard, and David C. Joy, editors. *Introduction to Electron Holography*. Springer US, 1999.

[2] D. Gabor. A New Microscopic Principle. *Nature*, May 1948.

[3] Akira Tonomura. *Electron Holography*. Springer Series in Optical Sciences. Springer-Verlag, Berlin Heidelberg, 2 edition, 1999.

[4] Martin Hÿtch, Florent Houdellier, Florian Hüe, and Etienne Snoeck. Nanoscale holographic interferometry for strain measurements in electronic devices. *Nature*, 453(7198):1086–1089, June 2008.

[5] M Gajdardziska-Josifovska and M.R. McCartney. Elimination of thickness dependence from medium resolution electron holograms. *Ultramicroscopy*, 53(3):291, March 1994.

[6] Jing Li, M.R McCartney, and David J. Smith. Semiconductor dopant profiling by off-axis electron holography. *Ultramicroscopy*, 94(2):149, February 2003.

[7] Ludvig de Knoop, Florent Houdellier, Christophe Gatel, Aurélien Masseboeuf, Marc Monthioux, and Martin Hÿtch. Determining the work function of a carbon-cone cold-field emitter by in situ electron holography. *Micron*, 63:2, August 2014.

[8] Christophe Gatel, Francisco Javier Bonilla, Anca Meffre, Etienne Snoeck, Bénédicte Warot-Fonrose, Bruno Chaudret, Lise-Marie Lacroix, and Thomas Blon. Size-specific spin configurations in single iron nanomagnet: From flower to exotic vortices. *Nanoletters*, 15(10):6952, 2015.

[9] C. Gatel, A. Lubk, G. Pozzi, E. Snoeck, and M. Hytch. Counting Elementary Charges on Nanoparticles by Electron Holography. *Phys. Rev. Lett.*, 111(2):025501–, July 2013.

[10] L. de Knoop, C. Gatel, F. Houdellier, M. Monthioux, A. Masseboeuf, E. Snoeck, and M. J. Hÿtch. Low-noise cold-field emission current obtained between two opposed carbon cone nanotips during in situ transmission electron microscope biasing. *Applied Physics Letters*, 106(26):263101, June 2015.

[11] Vladimir A. Lobastov, Ramesh Srinivasan, and Ahmed H. Zewail. Four-dimensional ultrafast electron microscopy. *Proceedings of the National Academy of Sciences of the United States of America*, 102(20):7069–7073, May 2005.

[12] Ahmed H. Zewail. 4D ultrafast electron diffraction, crystallography, and microscopy. *Annual Review of Physical Chemistry*, 57:65–103, 2006.

[13] Armin Feist, Nora Bach, Nara Rubiano da Silva, Thomas Danz, Marcel Möller, Katharina E. Priebe, Till Domröse, J. Gregor Gatzmann, Stefan Rost, Jakob Schauss, Stefanie Strauch, Reiner Bormann, Murat Sivis, Sascha Schäfer, and Claus Ropers. Ultrafast transmission electron microscopy using a laser-driven field emitter: Femtosecond resolution with a high coherence electron beam. *Ultramicroscopy*, 176(Supplement C):63–73, May 2017.

[14] F. Houdellier, G. M. Caruso, S. Weber, M. Kociak, and A. Arbouet. Development of a high brightness ultrafast Transmission Electron Microscope based on a laser-driven cold field emission source. *Ultramicroscopy*.

[15] Arnaud Arbouet, Giuseppe M. Caruso, and Florent Houdellier. Chapter One - Ultrafast Transmission Electron Microscopy: Historical Development, Instrumentation, and Applications. In *Advances in Imaging and Electron Physics*, volume 207, pages 1–72. Elsevier, January 2018.

[16] Giuseppe Mario Caruso, Florent Houdellier, Pierre Abeilhou, and Arnaud Arbouet. Development of an ultrafast electron source based on a cold-field emission gun for ultrafast coherent TEM. *Applied Physics Letters*, 111(2):023101, July 2017.

[17] Dominik Ehberger, Jakob Hammer, Max Eisele, Michael Krüger, Jonathan Noe, Alexander Högele, and Peter Hommelhoff. Highly Coherent Electron Beam from a Laser-Triggered Tungsten Needle Tip. *Physical Review Letters*, 114(22):227601, June 2015.

[18] F. J. García de Abajo and M. Kociak. Electron energy-gain spectroscopy. *New Journal of Physics*, 10(7):073035, 2008.

[19] Giuseppe Mario Caruso, Florent Houdellier, Sebastien Weber, and Arnaud Arbouet. *submitted*.

[20] Alex Harscher and Hannes Lichte. Experimental study of amplitude and phase detection limits in electron holography. *Ultramicroscopy*, 64(1):57–66, August 1996.

[21] W. J. de Ruijter and J. K. Weiss. Detection limits in quantitative off-axis electron holography. *Ultramicroscopy*, 50(3):269–283, August 1993.

[22] Michael Lehmann. Influence of the elliptical illumination on acquisition and correction of coherent aberrations in high-resolution electron holography. *Ultramicroscopy*, 100(1):9–23, July 2004.

[23] Shery L. Y. Chang, Christian Dwyer, Chris B. Boothroyd, and Rafal E. Dunin-Borkowski. Optimising electron holography in the presence of partial coherence and instrument instabilities. *Ultramicroscopy*, 151:37–45, April 2015.

[24] Victor Boureau, Robert McLeod, Benjamin Mayall, and David Cooper. Off-axis electron holography combining summation of hologram series with double-exposure phase-shifting: Theory and application. *Ultramicroscopy*, 193:52–63, October 2018.

[25] C. Gatel, J. Dupuy, F. Houdellier, and M. J. Hÿtch. Unlimited acquisition time in electron holography by automated feedback control of transmission electron microscope. *Applied Physics Letters*, 113(13):133102, September 2018.